14th International Symposium on Turbulence and Shear Flow Phenomena (TSFP14)
Heidelberg, Germany, July 28–31, 2026

STATISTICALLY STATIONARY RAYLEIGH–TAYLOR TURBULENCE

Chian Yeh Goh
Department of Mechanical and Civil Engineering
California Institute of Technology
1200 E. California Blvd., Pasadena, CA 91125
cgoh@caltech.edu

Guillaume Blanquart
Department of Mechanical and Civil Engineering
California Institute of Technology
1200 E. California Blvd., Pasadena, CA 91125
g.blanquart@caltech.edu

ABSTRACT

We propose a computational framework for simulating self-similar Rayleigh–Taylor (RT) turbulence in a statistically stationary manner. The governing equations for the statistically stationary RT (SRT) configuration are derived from the Navier-Stokes equations first by a rescaling of the physical variables into similarity variables, followed by simplifications of the transformed equations. Direct numerical simulations of the SRT configuration at different aspect ratios produce a range of statistics similar to late-time temporally growing RT (TRT) flow under varying initial conditions. At a specific aspect ratio $\lambda = 1.7$, a minimal flow unit is identified for self-similar RT turbulence, which incurs a significantly lower cost than equivalent TRT simulations, with improved statistical convergence. Results from the statistically stationary minimal flow unit agree well with self-similar TRT data across Reynolds and Atwood numbers. Finally, we examine the known breakdown of the classical scaling law $h \propto Agt^2$ under non-Boussinesq conditions, and propose an alternative scaling $h \propto (\ln R)gt^2$, which leads to an improved collapse of RT data across Atwood numbers.

INTRODUCTION

The Rayleigh–Taylor instability is observed in many flow applications, including atmospheric science, astrophysics, and inertial confinement fusion. When a heavier fluid of density ρ_H sits atop a lighter fluid of density ρ_L in the presence of gravity g, linear instabilities can be triggered by small perturbations, leading to nonlinear effects and the development of a turbulent mixing layer. In an infinitely large domain, it is believed that the temporally growing RT (TRT) mixing layer eventually attains self-similar growth. Using dimensional arguments, Youngs (1984) proposed that the height $h(t)$ grows as $h = F(R)gt^2$, where $\dot{h} = \mathrm{d}h/\mathrm{d}t$ and $F(R)$ is an unspecified function of the density ratio $R = \rho_H/\rho_L$. In the Boussinesq limit (i.e. $R \approx 1$), Ristorcelli & Clark (2004) derived an expression for the growth rate as

$$\dot{h}^2 = 4\alpha Agh \tag{1}$$

where $\mathrm{A} = \Delta\rho/(\rho_H + \rho_L)$ is the Atwood number, $\Delta\rho = \rho_H - \rho_L$, and α is a dimensionless growth parameter whose value depends on the specific choice of height definition.

While Eq. (1) suggests that α is a theoretical constant, practically observed values, α_{obs}, appear to be influenced by several factors, taking a dependence of the form $\alpha_{\mathrm{obs}} = f(\mathrm{Re}(t), h(t)/\ell_I, \mathrm{A}, \mathrm{Sc})$, where $\mathrm{Re}(t) = h\dot{h}/\nu$ is the Reynolds number, ℓ_I is a characteristic lengthscale of the initial perturbations, and Sc is the Schmidt number. In this work, we consider only the effects of A, Re, and the initial conditions.

The sensitivity of α_{obs} to the initial conditions (Ramaprabhu & Andrews, 2004; Mueschke & Schilling, 2009; Ramaprabhu *et al.*, 2005; Banerjee & Andrews, 2009; Youngs, 2013) is primarily due to the breakdown of the infinite-domain and late-time assumptions underlying Eq. (1). The late-time assumption implies that $\mathrm{Re}(t), h(t)/\ell_I \gg 1$, or equivalently, $h(t) \gg \ell_I, \eta$, where η is the Kolmogorov lengthscale. To approximate an infinite domain, the physical domain size L should satisfy $L \gg h(t) \gg \ell_I, \eta$. In most experiments, the magnitude of ℓ_I is difficult to control, and they tend to be comparable in magnitude to the domain size L. While direct numerical simulations (DNS) of the TRT configuration have successfully yielded time-independent α values (Cabot & Cook, 2006), they are computationally expensive and the effect of the domain boundaries remain uncertain.

Additionally, the influence of initial conditions and scale separation are intrinsically coupled in TRT flows, where both conditions $h(t) \gg \ell_I$ and $h(t) \gg \eta(t)$ are consistent with late-time conditions but cannot be studied independently. Their relative importance remains an open question.

The observed dependence of α on the Atwood number (Dimonte & Schneider, 2000; Banerjee *et al.*, 2010; Youngs, 2013; Zhou & Cabot, 2019) is not unexpected, since Eq. (1) was derived in the Boussinesq limit, and is not expected to hold at finite Atwood numbers. Beyond simple data regression, no functional form for $\alpha(\mathrm{A})$ has been derived for non-Boussinesq flows ($0 < \mathrm{A} < 1$). There are far fewer DNS studies in this flow regime, perhaps due to the fact that larger Atwood number RT flows take longer to converge to self-similarity, which further exacerbates the late-time computational demands.

To overcome some of the computational challenges associated with the traditional TRT configuration, a statistically stationary RT (SRT) flow configuration is proposed (Goh & Blanquart, 2025). In this work, we present its formulation, discuss its properties, and leverage its computational efficiency to answer some of the physics questions mentioned above.

MATHEMATICAL DESCRIPTION

Governing equations

The temporally growing RT configuration, described by the physical coordinates $(t, \hat{\mathbf{x}}, \hat{\mathbf{u}})$, is governed by the continuity, momentum, and scalar transport equations, written succinctly as $\{\mathsf{C}, \mathsf{M}_i, \mathsf{S}\}(t, \hat{\mathbf{x}}, \hat{\mathbf{u}}) = 0$, where

$$\mathsf{C}(t, \hat{\mathbf{x}}, \hat{\mathbf{u}}) = \frac{\partial \rho}{\partial t} + \frac{\partial \rho \hat{u}_j}{\partial \hat{x}_j} \tag{2}$$

$$\mathsf{M}_i(t, \hat{\mathbf{x}}, \hat{\mathbf{u}}) = \frac{\partial \rho \hat{u}_i}{\partial t} + \frac{\partial \rho \hat{u}_i \hat{u}_j}{\partial \hat{x}_j} + \frac{\partial p}{\partial \hat{x}_i} - \frac{\partial \hat{\tau}_{ij}}{\partial \hat{x}_j} + \rho g \delta_{2i} \tag{3}$$

$$\mathsf{S}(s, \hat{\mathbf{x}}, \hat{\mathbf{u}}) = \frac{\partial \rho Y}{\partial t} + \frac{\partial \rho Y \hat{u}_j}{\partial \hat{x}_j} - \frac{\partial}{\partial \hat{x}_j}\left(\rho D \frac{\partial Y}{\partial \hat{x}_j}\right) \tag{4}$$

Here ρ is density, $\hat{u}_i$ velocity, p pressure, D diffusivity, $\hat{\tau}_{ij}$ the shear stress tensor, and Y the mass fraction of the heavy fluid. In the low-Mach-number formulation, the mass fraction is uniquely related to density via the equation of state, $\rho(Y) = \rho_H \rho_L / (\rho_H - Y \Delta\rho)$.

Inspired by the self-similar nature of late-time RT growth, the governing equations for the SRT configuration are derived from the TRT equations through two main steps. First, the vertical coordinate $\hat{x}_2$ and velocities $\hat{u}_i$ are rescaled by the mixing layer height $q(t)$ and its derivative $\dot{q}(t)$, respectively, to yield

$$s = t, \quad x_i = \delta_{2i} \frac{q(t)}{q(t_0)} \hat{x}_i, \quad u_i = \frac{\dot{q}(t)}{\dot{q}(t_0)} \hat{u}_i \tag{5}$$

where $(s, \mathbf{x}, \mathbf{u})$ are the transformed coordinates and t_0 is a specific time. Substituting Eq. (5) into Eqs. (2)–(4) yields

$$\mathsf{C}(t, \hat{\mathbf{x}}, \hat{\mathbf{u}}) = \mathsf{C}(s, \mathbf{x}, \mathbf{u}) - \frac{\dot{q}(t)}{q(t)} y \frac{\partial \rho}{\partial y} + \ldots \tag{6}$$

$$\mathsf{M}_i(t, \hat{\mathbf{x}}, \hat{\mathbf{u}}) = \mathsf{M}_i(s, \mathbf{x}, \mathbf{u}) - \frac{\dot{q}(t)}{q(t)} y \frac{\partial \rho u_i}{\partial y} + \frac{\ddot{q}(t)}{\dot{q}(t)} \rho u_i + \ldots \tag{7}$$

$$\mathsf{S}(t, \hat{\mathbf{x}}, \hat{\mathbf{u}}) = \mathsf{S}(s, \mathbf{x}, \mathbf{u}) - \frac{\dot{q}(t)}{q(t)} y \frac{\partial \rho Y}{\partial y} + \ldots \tag{8}$$

where the original TRT dynamics (LHS) can be represented in the transformed coordinate system (RHS) by the same governing equations but with additional source terms which restrict the growth of the mixing layer. This transformation is purely algebraic and Eqs. (6)–(8) can theoretically be solved in the transformed variables to simulate a TRT flow with a statistically stationary height. However, $\mathrm{Re}(t)$ will continue to grow as the rescaled smallest scales get progressively smaller like $\eta/h \sim \mathrm{Re}^{-3/4}$. Such a simulation offers no computational advantage relative to traditional TRT simulations.

In order to achieve stationarity at all lengthscales, a crucial second step involves evaluating Eqs. (6)–(8) at a specified time $t = t_0$, which simplifies them to

$$\mathsf{C}(s, \mathbf{x}, \mathbf{u}) = \frac{y}{\tau_0} \frac{\partial \rho}{\partial y} \tag{9}$$

$$\mathsf{M}_i(s, \mathbf{x}, \mathbf{u}) = \frac{y}{\tau_0} \frac{\partial \rho u_i}{\partial y} - \frac{\rho u_i}{2\tau_0} \tag{10}$$

$$\mathsf{S}(s, \mathbf{x}, \mathbf{u}) = \frac{y}{\tau_0} \frac{\partial \rho Y}{\partial y} \tag{11}$$

where $\tau_0 = q(t_0)/\dot{q}(t_0)$. Here we have assumed that (I) the simplified governing equations approximate RT turbulence well in the vicinity of $t = t_0$, and (II) the physical RT height grows like $q \sim t^2$. These are the final form of the SRT equations; they resemble the TRT equations but with additional source terms that depend on a single parameter τ_0. The timescale τ_0 determines the magnitude of the RHS source terms that counteract the TRT growth associated with the LHS terms, directly controlling the stationary height.

In a temporally self-similar flow, all large-scale height definitions $h_i(t)$ scale proportionally to $q(t)$ and to each other, yielding the physical interpretation of the SRT timescale parameter as $[1/\tau_0]_{\mathrm{SRT}} = [\dot{h}_i(t_0)/h_i(t_0)]_{\mathrm{TRT}}$. Although the height of the SRT mixing layer does not grow in the transformed coordinates, the TRT-equivalent growth is captured by the SRT parameter τ_0. Substituting this relation for τ_0 into Eq. (1), a TRT-equivalent growth parameter can be computed from the SRT flow configuration as

$$\alpha_i = \frac{h_i}{4Ag\tau_0^2}. \tag{12}$$

Inputs

Unlike TRT flow, SRT flow evolves over long simulation times and is assumed to be independent of its initial conditions after sufficiently many integral timescales; this is verified later. At the same time, long simulation times may lead to box-filling effects and a dependence on the domain size. Hence, the SRT configuration is fully defined by fluid properties (ρ_H, ρ_L, ν, D), gravity g, the lateral domain size L^*, and the stationary mixing layer height h_1. Here the specific definition $h_1 = \int 4\bar{X}(1 - \bar{X})\mathrm{d}y$ is used, where $\bar{X}$ is the mean mole fraction. Applying the Buckingham-Pi theorem to the seven input parameters, the SRT configuration is fully specified by four non-dimensional numbers,

$$\mathrm{A} = \frac{\rho_H - \rho_L}{\rho_H + \rho_L}, \quad \mathrm{Sc} = \frac{\nu}{D}, \quad \mathrm{Gr} = \frac{Agh_1^3}{\nu^2}, \quad \lambda = \frac{h_1}{L^*} \tag{13}$$

where Gr is the Grashof number and λ is the aspect ratio. The Grashof number characterizes the relative effects of large-scale buoyancy and molecular-scale viscosity, and scales approximately with $\mathrm{Gr} \sim \mathrm{Re}^2$. While Gr is listed as the input parameter here, subsequent results are presented in terms of the Reynolds number, $\mathrm{Re} = H^2/\tau_0\nu$, where $H = y(\bar{X} = 0.99) - y(\bar{X} = 0.01)$, which is more common in the broader turbulence literature. The aspect ratio λ describes the geometry of the integral scales, where the largest vertical scales are confined by h_1 and the horizontal scales by L^*.

In the present work, $\mathrm{Sc} = 1$ is kept constant, and the effects of initial conditions, λ, Gr (or Re), and A are investigated. The input parameters are summarized in Table 1. Direct numerical simulations are performed using the computational solver NGA (Desjardins *et al.*, 2008) with the Bounded Cubic Hermite interpolation (BCH) scheme for scalar transport (Verma *et al.*, 2014). The implementation of the additional source terms on the RHS of Eqs. (9)–(11) is described in Goh & Blanquart (2025). The simulation configuration is periodic in x_1 and x_3, with Dirichlet boundary conditions in x_2. The computational grid has a uniformly spaced core region, with a vertically stretched grid in regions far from the mixing layer core. A minimum resolution of $\kappa_{\max}\eta \gtrsim 3$ is maintained across all simulations.

Table 1. Summary of simulation cases

Label	A	λ	Gr (approx.)	I.C.
I	0.5	1.7	10^7	vary
L	0.5	0.8–2.6	10^7	other SRT
G	0.5	1.7	$10^5 - 10^8$	other SRT
A	0.01–0.8	1.7	10^7	other SRT

RESULTS

The results from the simulations listed in Table 1 are presented and discussed below. The temporal properties of the SRT flow configuration are discussed, followed by the effect of the aspect ratio, Reynolds number, and Atwood number.

Statistical stationarity

Set I consists of three SRT simulations with different initial conditions. The first case is an initially perturbed, planar interface that is evolved in time using the SRT equations. The second case is initialized with the full 3D flow field of a separate TRT simulation at a similar target height. The last is initialized with interpolated data of a different SRT flow at a similar height but lower Reynolds number.

The temporal evolution of the large-scale height, h_1, and the Kolmogorov scale, $\eta_{\min} = \min_y(\bar{\rho}\nu^3/\langle\tau_{ij}(\partial u_i/\partial x_j)\rangle)^{1/4}$, are shown in Fig. 1. All three cases show stationarity in both the large and small scales after $s \sim \tau_0$, which demonstrates that the SRT flow configuration can be run for arbitrarily long times on the same grid, generating many flow realizations that lead to excellent statistical convergence. As expected, the stationary state is fully defined by the four parameters in Eq. (13) and does not depend on the initial conditions. Hence, thoughtful flow initialization strategies may be adopted to speed up convergence to the target flow state.

In the following sections, all reported SRT results reflect temporal averages of the converged stationary state.

Effect of aspect ratio

The effect of the aspect ratio λ on the growth and mixedness parameters is shown for Set L in Fig. 2. Here we choose a specific definition of the growth parameter α_p based on $h_p = \int 2\min(\bar{X}, 1-\bar{X})\,\mathrm{d}y$, and a corresponding definition for mixedness, $\Xi = (\int\langle\min(X, 1-X)\rangle\,\mathrm{d}y)/(\int\min(\bar{X}, 1-\bar{X})\,\mathrm{d}y)$, in order to facilitate comparison with TRT results from Cabot & Cook (2006). As λ increases, α decreases and Ξ grows. At $\lambda \approx 1.7$, however, both parameters agree well with the DNS results for self-similar TRT flow from Cabot & Cook (2006).

A comparison of the density field between self-similar TRT and SRT ($\lambda = 1.7$) at similar Reynolds numbers is shown in Fig. 3. The two flows are qualitative similar, although the SRT configuration isolates a single large-scale structure using a much smaller lateral domain size, $L^* \approx L/4$. For self-similar TRT flows, the domain size L exerts no dynamical significance

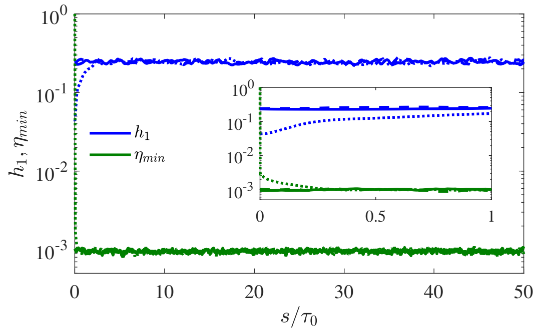

Figure 1. Time evolution of h_1 (blue) and $\eta_{\min}$ (green) for the SRT configuration. Line styles correspond to different initial conditions: planar interface (dotted); TRT flow field at similar height (dashed); lower Gr SRT flow field at similar height (solid). Inset zooms in on initial transients.

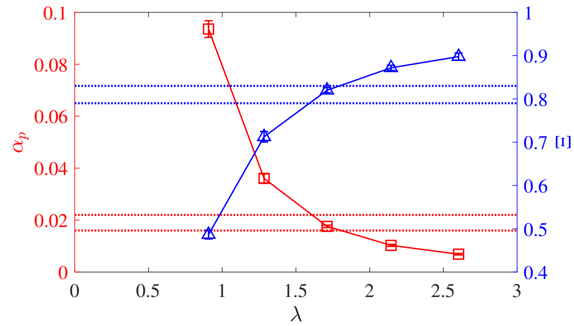

Figure 2. Effect of aspect ratio λ on growth parameter α_p (red squares) and mixedness Ξ (blue triangles). The dotted lines represent the range of values from self-similar TRT DNS (Cabot & Cook, 2006; Goh & Blanquart, 2025).

within the finite time of interest, and the large-scale structure evolves entirely through the coupling of smaller structures. During self-similar growth, the aspect ratio of *integral* length-scales remains approximately constant across A and Re (Zhou & Cabot, 2019). The SRT configuration enforces this stationarity in aspect ratio by directly enforcing height stationarity in the vertical direction and confining the corresponding horizontal scale using the domain size L^*, representing exactly one unit of the large-scale structure.

The effect of SRT lateral confinement is demonstrated by the spectra of SRT $\lambda = 1.7$ and the equivalent TRT flow, shown in Fig. 4. The SRT configuration captures a small-scale cascade similar to TRT flow, but without resolving length scales larger than the peak of the energy spectrum, functioning as a minimal flow unit (MFU) for RT turbulence. Consequently, it requires only one-sixteenth of the grid cells required by a typical TRT configuration of a similar Reynolds number. In addition to α_p and Ξ, Goh & Blanquart (2025) demonstrated that many other global and 1D quantities from SRT flow show strong agreement with self-similar TRT results (Cabot & Cook, 2006; Livescu *et al.*, 2009) at $\lambda \approx 1.7$.

Besides the (mode-coupling) self-similar limit represented by $\lambda = 1.7$, SRT configurations of $\lambda < 1.7$ may also represent other RT regimes of interest. Smaller aspect ratios yield larger α_p and smaller Ξ, an outcome similar to late-time TRT values that are evolved from large-wavelength initial perturbations. These late-time TRT cases are not strictly

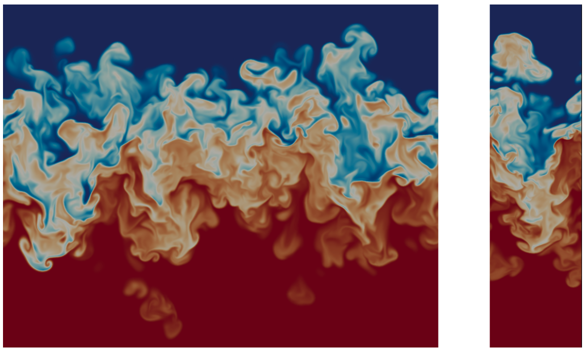

Figure 3. Comparison of TRT (left) and SRT (right) density field for Re $\approx$ 6400. Reproduced with permission from Goh & Blanquart (2025)

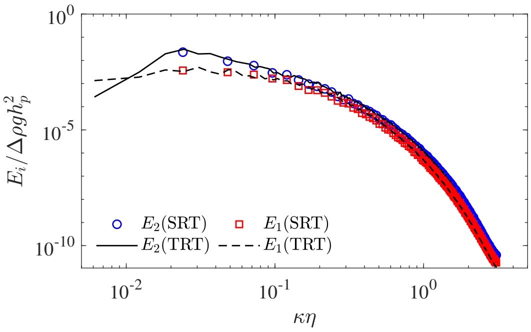

Figure 4. Comparison of TRT (lines) and SRT $\lambda = 1.7$ (markers) spectra at $y = 0$ for Re $\approx$ 6400. Adapted from Goh & Blanquart (2025)

self-similar as they depend on a second length scale ℓ_I (in addition to $h(t)$), and their α values exhibit slow temporal variation after transition to turbulence (Youngs, 2013). Nonetheless, α values are often extracted, and we refer to them more broadly as late-time growth parameters. Figure 5 compares the SRT cases from Set L with late-time TRT values from the literature across a range of initial conditions (IC), showing that similar (α_p, Ξ) combinations are produced. Generally, late-time TRT behavior is characterized by $(\mathrm{A}, \mathrm{Sc}, \mathrm{Re}, h(t)/\ell_I)$, while SRT flow is defined by $(\mathrm{A}, \mathrm{Sc}, \mathrm{Re}, \lambda)$. It appears that SRT configurations of $\lambda < 1.7$ may approximate the quasi-self-similar late-time dynamics of TRT flows originating from large-wavelength perturbations, where the domain-imposed λ in SRT can approximate the effects of the IC-imposed $h(t)/\ell_I$ in TRT flows.

A thorough investigation of the $\lambda < 1.7$ cases is left for future work. The remainder of this study focuses exclusively on the strict self-similar case corresponding to $\lambda = 1.7$.

Effect of Reynolds number

In TRT flow, the effect of scale separation ($h(t)/\eta$) and initial conditions (or $h(t)/\ell_I$) are inherently linked in time — any $\alpha(\mathrm{Re}(t))$ history contains both effects. In contrast, converged SRT flow is independent of its initial conditions and the influence of scale separation can be examined in isolation. The effect of Reynolds number on α_p, Ξ, and η is shown in Fig. 6 for both SRT (Set G) and TRT flow. Both the α and Ξ values for SRT approach the high-Re limit in a smooth monotonic fashion, which suggests that the large variations in the early-time TRT results are related to the finite-time influence

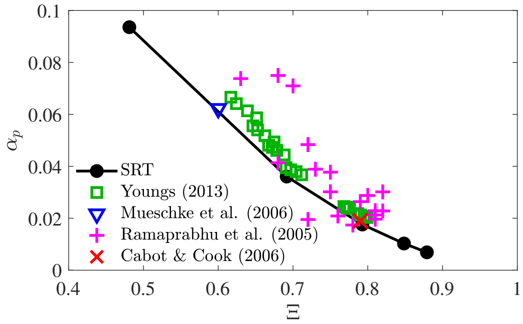

Figure 5. Relationship between growth parameter α_p and mixedness Ξ as λ is varied. SRT results (black circles) are compared with late-time TRT results with different initial perturbations (Ramaprabhu *et al.*, 2005; Mueschke *et al.*, 2006; Cabot & Cook, 2006; Youngs, 2013)

of the initial conditions, rather than scale separation effects.

The variation in α and Ξ values for SRT cases where Re < 2000 can be attributed to changes in the relative influence of viscous/diffusive effects with respect to the buoyancy-driven inertial dynamics. Although these variations in global flow properties are apparent, the one-dimensional profiles of planar-averaged mole fraction $\langle X \rangle = (\bar{\rho} - \rho_L)/\Delta\rho$, mass flux $\langle \rho v \rangle$, and turbulent kinetic energy $\langle \rho k \rangle$ seem to exhibit a strong collapse across Re, after they are normalized by the appropriate global quantities, demonstrating that the nature of local turbulent mixing is qualitatively similar across all Reynolds numbers.

Finally, the existence of unique SRT solutions for all Re and their smooth convergence to the high-Re limit make the SRT flow configuration an excellent test bed for incremental efforts in model development and testing.

Effect of Atwood number

Lastly, the effect of Atwood number is studied. Growth parameters α_1 (defined in terms of h_1) are computed from Set A and are shown in the top panel of Fig. 8, alongside other sources of TRT data from experiments (Dimonte & Schneider, 2000; Banerjee *et al.*, 2010) and numerical simulations (Youngs, 2013; Zhou & Cabot, 2019). As each study had different initial conditions and employed different height definitions, α_i values are not expected to be consistent across studies. Nonetheless, it is evident that all studies report an increase of α_i with A, illustrating the breakdown of Eq. (1) scaling in non-Boussinesq conditions.

We propose an alternative scaling law to Eq. (1) for finite-Atwood-number regimes by leveraging data from the SRT flow configuration. A more rigorous derivation is presented in Goh *et al.* (2026) but an outline of the steps are presented here.

First, we postulate that the TRT-equivalent growth of the SRT mixing layer scales with a volume-averaged turbulent velocity fluctuation, i.e.,

$$\left(\frac{h_1}{\tau_0}\right)^2 \propto \int \tilde{k}\,\mathrm{d}\left(\frac{y}{h_1}\right) = \frac{1}{h_1}\int \frac{\langle \rho k \rangle}{\mathrm{d}\bar{\rho}/\mathrm{d}y}\,\mathrm{d}(\ln\bar{\rho}), \qquad (14)$$

where the Favre-averaged TKE is expanded as $\tilde{k} = \langle \rho k \rangle/\bar{\rho} = \langle \rho k \rangle(\mathrm{d}\ln\bar{\rho}/\mathrm{d}\bar{\rho}) = [\langle \rho k \rangle/(\mathrm{d}\bar{\rho}/\mathrm{d}y)](\mathrm{d}\ln\bar{\rho}/\mathrm{d}y)$.

To evaluate Eq. (14), we examine the mean density and TKE profiles, which are normalized and shown in Fig. 9. Although there are discrepancies near the mixing layer edges,

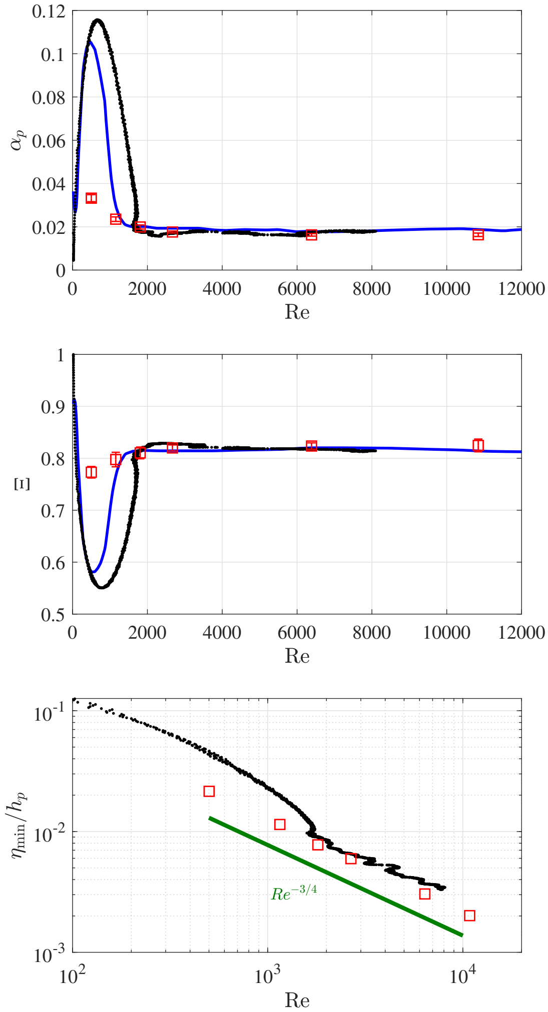

Figure 6. Effect of Re on growth parameter, mixedness, and Kolmogorov scale. SRT results (red squares) are compared with TRT results from Cabot & Cook (2006) (blue line) and Goh & Blanquart (2025) (black line). Reproduced with permission from Goh & Blanquart (2025).

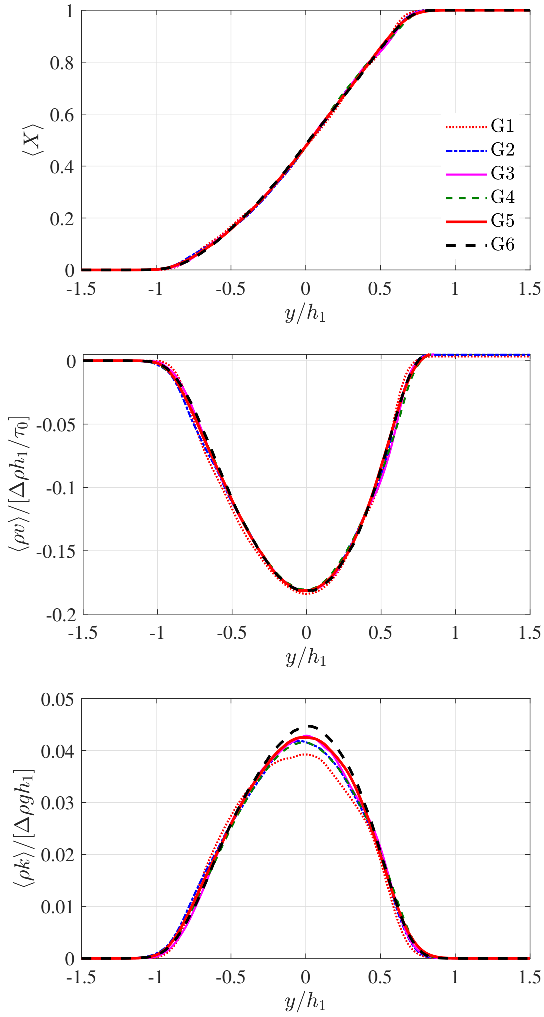

Figure 7. Effect of Re on the mean mole fraction, mass flux, and turbulent kinetic energy. Cases G1–G6 correspond to Re $\approx$ 500, 1200, 2700, 6400, and 10800, respectively. Reproduced with permission from Goh *et al.* (2026).

both the mean density and TKE exhibit a strong collapse across Atwood numbers after normalization. Notably, the mean mole fraction and normalized TKE resemble error and Gaussian functions, respectively. Applying these approximations, the ratio $\langle \rho k \rangle / (\mathrm{d}\bar{\rho}/\mathrm{d}y)$ is treated as constant across the mixing layer, and Eq. (14) can be simplified as $(h_1/\tau_0)^2 = \alpha_1^* C g h_1 \ln R$, where $C = 1/2$ is chosen to enforce $\alpha_1^* = \alpha_1$ in the Boussinesq ($A \to 0$) limit. The final scaling for the mixing layer height is

$$\dot{h}^2 = 2\alpha_1^* \ln R g h. \tag{15}$$

Using this scaling, the α_i values from Fig. 8(a) are converted to $\alpha_i^* = 2\alpha A/(\ln R)$ and shown in Fig. 8(b). Within each study, α_i^* remains nearly constant for the range of Atwood numbers considered, suggesting that $\ln R$ is a more complete representation of density effects in a variable-density RT flow than the Atwood number.

CONCLUSION

In this work, we present the framework for a statistically stationary RT configuration and identify a minimal flow unit corresponding to self-similar RT turbulence. Leveraging this computationally efficient framework, the effects of initial conditions and turbulence scale separation in RT flow are studied independently, revealing the possibility of self-similar RT mixing at Reynolds numbers much lower than previously observed in TRT flows. Finally, we apply the framework to investigate the effect of Atwood number on the growth parameter. We propose and verify that, under non-Boussinesq conditions, the mixing layer height scales more completely with $\ln(\rho_H/\rho_L)$ than with the Atwood number.

REFERENCES

Banerjee, A. & Andrews, M. J. 2009 3D simulations to investigate initial condition effects on the growth of Rayleigh–Taylor mixing. *Intl J. Heat Mass Transfer* **52** (17-18), 3906–3917.

Banerjee, A., Kraft, W. N. & Andrews, M. J. 2010 Detailed measurements of a statistically steady Rayleigh–Taylor

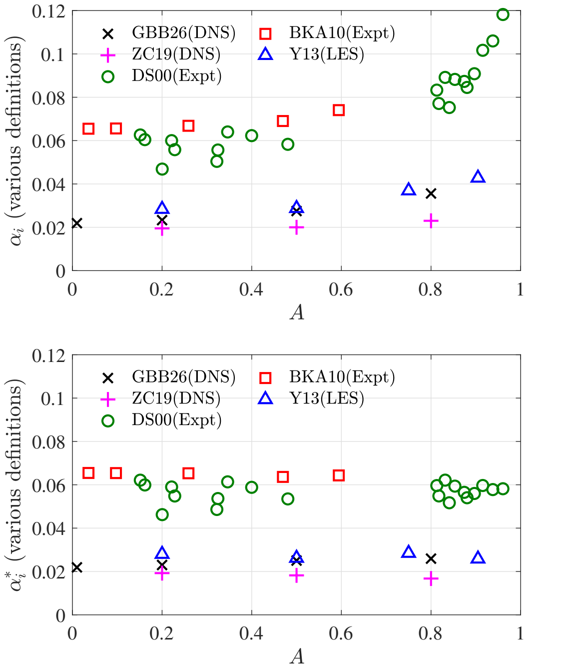

Figure 8. Effect of A on (top) the traditional growth parameter, $\alpha_i = \dot{h}_i^2/(4Agh_i)$; and (bottom) the effective growth parameter, $\alpha^* = \dot{h}_i^2/(2\ln Rgh_i)$. Studies (Dimonte & Schneider, 2000; Banerjee *et al.*, 2010; Youngs, 2013; Zhou & Cabot, 2019; Goh *et al.*, 2026) use different height definitions and have different initial conditions. Adapted from Goh *et al.* (2026).

mixing layer from small to high Atwood numbers. *J. Fluid. Mech.* **659**, 127–190.

Cabot, W. H. & Cook, A. W. 2006 Reynolds number effects on Rayleigh–Taylor instability with possible implications for type-Ia supernovae. *Nat. Phys.* **2**, 562 – 568.

Desjardins, O., Blanquart, G., Balarac, G. & Pitsch, H. 2008 High order conservative finite difference scheme for variable density low Mach number turbulent flows. *J. Comput. Phys.* **227** (15), 7125–7159.

Dimonte, G. & Schneider, M. 2000 Density ratio dependence of Rayleigh—Taylor mixing for sustained and impulsive acceleration histories. *Phys. Fluids* **12** (2), 304–321.

Goh, C. Y. & Blanquart, G. 2025 A statistically stationary minimal flow unit for self-similar Rayleigh–Taylor turbulence in the mode-coupling limit. *J. Fluid Mech.* **1002**, A19.

Goh, C. Y., Brito Matehuala, D. & Blanquart, G. 2026 Self-similar scaling of variable-density Rayleigh–Taylor turbulence. *J. Fluid Mech.* **1030**, A14.

Livescu, D., Ristorcelli, J. R., Gore, R. A., Dean, S. H., Cabot, W. H. & Cook, A. W. 2009 High-Reynolds number Rayleigh—Taylor turbulence. *J. Turbul.* **10**, N13.

Mueschke, N. J., Andrews, M. J. & Schilling, O. 2006 Experimental characterization of initial conditions and spatio-temporal evolution of a small-Atwood-number Rayleigh–Taylor mixing layer. *J. Fluid Mech.* **567**, 27–63.

Mueschke, N. J. & Schilling, O. 2009 Investigation of Rayleigh–Taylor turbulence and mixing using direct numerical simulation with experimentally measured initial conditions. I. Comparison to experimental data. *Phys. Fluids* **21** (1), 014106.

Ramaprabhu, P. & Andrews, M. J. 2004 On the initialization of Rayleigh–Taylor simulations. *Phys. Fluids* **16** (8), L59–L62.

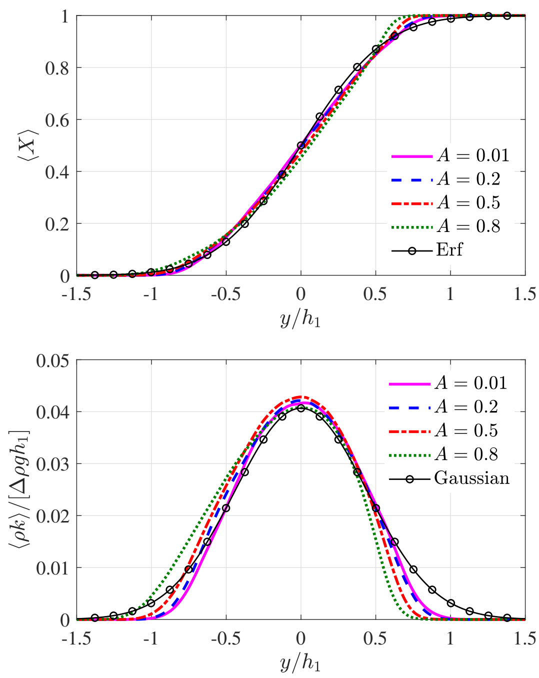

Figure 9. Effect of A on the mean mole fraction and turbulent kinetic energy. Adapted from Goh *et al.* (2026).

Ramaprabhu, P., Dimonte, G. & Andrews, M. J. 2005 A numerical study of the influence of initial perturbations on the turbulent Rayleigh–Taylor instability. *J. Fluid Mech.* **536**, 285–319.

Ristorcelli, J. R. & Clark, T. T. 2004 Rayleigh–Taylor turbulence: self-similar analysis and direct numerical simulations. *J. Fluid Mech.* **507**, 213–253.

Verma, S., Xuan, Y. & Blanquart, G. 2014 An improved bounded semi-Lagrangian scheme for the turbulent transport of passive scalars. *J. Comput. Phys.* **272**, 1–22.

Youngs, D. L. 1984 Numerical simulation of turbulent mixing by Rayleigh–Taylor instability. *Phys. D* **12** (1-3), 32–44.

Youngs, D. L. 2013 The density ratio dependence of self-similar Rayleigh–Taylor mixing. *Phil. Trans. R. Soc. Lond. A* **371** (2003), 20120173.

Zhou, Y. & Cabot, W. H. 2019 Time-dependent study of anisotropy in Rayleigh–Taylor instability induced turbulent flows with a variety of density ratios. *Phys. Fluids* **31** (8), 084106.